Published online 8 May 2017 *Nucleic Acids Research, 2017, Vol. 45, No. 11* ***6945–6959***
doi: 10.1093/nar/gkx324

RsgA couples the maturation state of the 30S ribosomal decoding center to activation of its GTPase pocket

Jorge Pedro López-Alonso[1,†], Tatsuya Kaminishi[1,†], Takeshi Kikuchi[2,†], Yuya Hirata[2], Idoia Iturrioz[1], Neha Dhimole[1], Andreas Schedlbauer[1], Yoichi Hase[2], Simon Goto[2], Daisuke Kurita[2], Akira Muto[2], Shu Zhou[1], Chieko Naoe[3], Deryck J. Mills[4], David Gil-Carton[1], Chie Takemoto[3], Hyouta Himeno[2,*], Paola Fucini[1,5] and Sean R. Connell[1,5,*]

[1]Molecular Recognition and Host-Pathogen Interactions, CIC bioGUNE, Bizkaia Technology Park, 48160 Derio, Spain, [2]Department of Biochemistry and Molecular Biology, Faculty of Agriculture and Life Science, Hirosaki University, Hirosaki, Aomori 036-8561, Japan, [3]Division of Structural and Synthetic Biology, RIKEN Center for Life Science Technology, 1-7-22 Suehiro-cho, Tsurumi, Yokohama 230-0045, Japan, [4]Max Planck Institute of Biophysics, Department of Structural Biology, Max-von-Laue-Straße 3, D-60438 Frankfurt am Main, Germany and [5]IKERBASQUE, Basque Foundation for Science, 48011 Bilbao, Spain

Received February 05, 2017; Revised March 28, 2017; Editorial Decision March 29, 2017; Accepted April 19, 2017

ABSTRACT

During 30S ribosomal subunit biogenesis, assembly factors are believed to prevent accumulation of misfolded intermediate states of low free energy that slowly convert into mature 30S subunits, namely, kinetically trapped particles. Among the assembly factors, the circularly permuted GTPase, RsgA, plays a crucial role in the maturation of the 30S decoding center. Here, directed hydroxyl radical probing and single particle cryo-EM are employed to elucidate RsgA´s mechanism of action. Our results show that RsgA destabilizes the 30S structure, including late binding r-proteins, providing a structural basis for avoiding kinetically trapped assembly intermediates. Moreover, RsgA exploits its distinct GTPase pocket and specific interactions with the 30S to coordinate GTPase activation with the maturation state of the 30S subunit. This coordination validates the architecture of the decoding center and facilitates the timely release of RsgA to control the progression of 30S biogenesis.

INTRODUCTION

The bacterial 70S ribosome is a large 2.4 MDa molecular machine responsible for protein synthesis that is composed of two subunits, the 30S and 50S subunits. The 30S subunit is assembled from an rRNA precursor and 21 ribosomal proteins (r-proteins, bS1–bS21) in a metabolically costly process termed ribosome biogenesis that is strictly regulated and responsible for cell growth. Although the 30S subunit can be reconstituted *in vitro* from only its constitutive components, the 16S rRNA and r-proteins uS2–bS21, in *Escherichia coli*, there is a growing list of accessory proteins, including at least five assembly factors and 15 modifying enzymes, involved in 30S biogenesis (1). Initially, the 30S assembly map (or Nomura assembly map) established the ordered and sequential fashion in which the r-proteins, categorized accordingly into primary, secondary, and tertiary binders, are assembled onto the ribosome under equilibrium conditions (2). The binding of r-proteins to the 16S rRNA is generally responsible for promoting long-range tertiary structure, while local secondary structure (i.e. helices) forms independently of r-proteins (3,4). Subsequent pulse-labeling based quantitative mass-spectrometry (PC/QMS) experiments have expanded on the Nomura assembly map by providing a kinetic description of 30S subunit assembly, showing that individual r-protein binding rates vary over two orders of magnitude and generally correspond to the binding order described in the classical Nomura assembly map (5). Importantly, this study and others (4–6) indicated that 30S assembly can follow multiple parallel pathways.

In line with the co-transcriptional nature of ribosome assembly, r-protein binding rates follow the 5′ to 3′ directionality of rRNA transcription, such that r-proteins bind

*To whom correspondence should be addressed. Tel: +34 946 572 529; Email: sean.connell@gmail.com
Correspondence may also be addressed to Hyouta Himeno. Tel: +81 172 39 3592; Fax: +81 172 39 3593; Email: himeno@hirosaki-u.ac.jp
†These authors contributed equally to this work as first authors.
Present address: Chieko Naoe, School of Pharmaceutical Sciences, Showa University, 1-5-8 Hatanodai, Shinagawa-ku, Tokyo 142-8555, Japan.

© The Author(s) 2017. Published by Oxford University Press on behalf of Nucleic Acids Research.
This is an Open Access article distributed under the terms of the Creative Commons Attribution License (http://creativecommons.org/licenses/by-nc/4.0/), which permits non-commercial re-use, distribution, and reproduction in any medium, provided the original work is properly cited. For commercial re-use, please contact journals.permissions@oup.com

rapidly to the 5′ 16S rRNA domain that forms the 30S body, and more slowly to the 3′ domain that forms the 30S head (5). This directionality has also been observed in time-resolved cryo-EM experiments where assembly intermediates from *in vitro* assembly experiments were visualized (6). This study, as well as subsequent studies with *in vivo* assembled intermediates, has shown that the earliest observed particles, Group I particles, show density corresponding to only the 30S 5'-body and central platform domains, while the 3'-head domain appears later, being either detached (Group II) or attached (Group III) to the 30S body (6,7). The fact that there are two 30S head positions seen in the assembly intermediates suggests that there are two alternative pathways for its maturation with the binding of r-protein S5 playing a role in promoting the attachment of the head by stabilizing the h1/h28 interface (7). In terms of r-proteins, the Group I particles lack, as expected, 3′-head domain binding proteins (uS2, uS3, uS7, uS9, uS10, uS13, uS14, uS19) as well as the 5′-body proteins, uS5 and uS12 (7). Note throughout the manuscript we use the r-protein naming convention described by Ban and colleagues (8) where the *u* and *b* prefix indicate proteins that are present in all three domains (universal) or are specific to bacteria, respectively. The Group II and III particles contain uS5 but remain deficient in the 5′-body protein, uS12 (7). Finally, the later stage Group IV and V particles, which are the most similar to the mature 30S subunit, are deficient in only uS2, uS3 and bS21 to varying extents.

Overall the folding of the 5′ and central domains is more robust than that of the 3′ domain possibly due to redundant, alternative assembly pathways, while assembly of the 3′ domain follows a more restrictive pathway that is susceptible to interference and kinetic traps (9), accounting for the higher number of ribosome assembly factors that intervene in its assembly. For example, in the 3′ head domain, the assembly factor RimM is proposed to avoid kinetic traps by holding the solvent side helices in a more open conformation, allowing h43 to be transcribed and core helices 31 and 43 to fold correctly (10). Similarly, RimP is suggested to avoid pathways leading to kinetically unfavorable Group II intermediates by facilitating the formation of a long-range pseudoknot interaction that lies at the core of the 30S decoding center to form the interface of the head and body domains (7). RbfA significantly affects the conformation of h44 and is thought to play a role in the maturation of this central pseudoknot region and 30S decoding centre, by directing the refolding of the 16S rRNA leader and h1 (10–12).

In this study, we focus on the role of the GTPase, RsgA (also called YjeQ/YloQ/CpgA) (13,14), a ribosome assembly factor that intervenes during the later stages of 30S maturation. RsgA is broadly conserved among bacteria (13,15), and deletion of the protein or inactivation of its GTPase activity strongly affects cell growth (14), ribosomal profiles (14,16,17), processing of 17S rRNA, a major precursor of 16S rRNA (14,18), peptidoglycan metabolism, cell morphology (19), and virulence in *Staphylococcus aureus* (20), suggesting its roles in ribosome biogenesis, bacterial survival and fitness (18). RsgA in the GTP form binds tightly to the 30S subunit, which also strongly stimulates its intrinsic GTPase activity (over 100-fold) (14,21,22). Since both the RbfA-releasing activity of RsgA and activation of its GTPase activity occur significantly on mature 30S subunit rather than on immature 30S subunits, RsgA is thought to act at nearly the last stage of 30S maturation (14,21,22). RsgA promotes dissociation of RbfA from the 30S subunit (21) and as such facilitates the docking of the penultimate 16S rRNA helix, h44, on to the body of the 30S subunit (23,24). Indeed, ribosomes purified from RsgA depleted strains (Δ*rsgA*) are characterized by a distorted decoding center where h44/h45/h24 are not juxtaposed, preventing these particles from associating with the 50S subunit and engaging in translation (25). Like other assembly factors, RsgA is assumed to facilitate 30S assembly by preventing and/or rescuing kinetically trapped 30S assembly intermediates (22,23,26) although the structural basis for this activity is unknown.

RsgA belongs to the TRAFAC class of GTPases that comprises translational factors and Ras-like proteins (15), and thus shares an evolutionarily conserved GTPase domain characterized by the presence of the G1–G5 motifs, which are critical for GTP/GDP binding, GTP-induced conformational changes and GTP hydrolysis (27). Interestingly, the GTPase motifs in RsgA are circularly permuted such that they follow a G4–G5–G1–G2–G3 order in the primary sequence instead of the sequential, G1–G2–G3–G4–G5, order. Accordingly, RsgA belongs to the subfamily of circularly permuted GTPases (CP-GTPase) alongside other ribosome biogenesis factors like RbgA(YlqF), YqeH and YawG, (15). In the case of RsgA, the CP-GTPase is preceded by a N-terminal oligonucleotide/oligosaccharide binding-fold domain (OB-domain) and followed by a zinc-binding domain (Zn-domain) on the C terminus (13,28,29). In GTPases, the loops containing the G2 and G3 motifs, designated switch 1 and switch 2, respectively, undergo a large conformational change upon GTP hydrolysis that is important for cellular function (27). In ribosome-dependent GTPases like EF-G and EF-Tu, the ribosome stimulates GTP hydrolysis by helping to position a catalytic residue in switch 2 (His84 in EF-Tu and His91 in EF-G), corresponding to Gln61 in the prototypical GTPase Ras, in a conformation suitable for coordinating the active site water (30). Notably, this residue in RsgA is substituted by a valine (Val270), which is typical of the so-called family of HAS-GTPases (Hydrophobic Amino acid Substituted for catalytic glutamine GTPases (31)). Because of this substitution, the HAS-GTPases are believed to use an alternative mechanism for GTP hydrolysis (31). For example, it has been suggested that the catalytic histidine residue in the circularly permuted HAS-GTPase RbgA originates from the outside of the switch 2 region, where His9 approaches the γ-phosphate group in a manner similar to the catalytic residue of EF-Tu (32). However, for RsgA and other ribosome-associated CP/HAS-GTPases, the structural foundation underlying the mechanism of GTP hydrolysis including the role of the ribosome in activation of the GTP pocket is unknown. In the case of RsgA, this stems from the fact that although RsgA has been studied both in its free form by X-ray crystallography and the ribosome-bound form by cryo-EM (23,28,29,33), the functionally important switch 1 region is disordered in the X-ray structures,

while the two cryo-EM structures reported, in addition to depicting RsgA in opposing orientations on the 30S, due to their lower resolution, lack the molecular details to understand the mechanism of GTP hydrolysis.

With the increased importance of ribosome biogenesis as a potential anti-microbial target, the chemical basis of RsgA activity becomes more important (34–36). Accordingly, in this study, we used advanced single particle cryo-EM and directed hydroxyl radical probing to characterize the interaction of RsgA in its GTP and GDP form with the 30S subunit. Taken together, the results elucidate the overall mode of interaction of RsgA with the 30S subunit and how it changes in response to the bound guanine nucleotide. Moreover, on the 30S subunit, the GTPase pocket of RsgA, including the functionally important switch 1 region, is ordered and observed in an activated state that is dependent on interactions with key features of the 30S mRNA/tRNA binding sites. The structure reveals that, unlike other TRAFAC-GTPases, the catalytic residue in RsgA originates in the switch 1 loop (His248) and therefore represents a mechanistic variation of the classical GTPase pocket. Elements of the 16S rRNA play a role in positioning this catalytic residue analogous to that played by the 23S rRNA in activating TRAFAC-GTPases like EF-Tu. Finally, the 30S–RsgA reconstruction provides structural evidence that RsgA has a role in destabilizing kinetically trapped assembly intermediate as it induces local conformational changes in the 30S structure and disrupts binding of uS2, uS3, uS12 and bS21.

MATERIALS AND METHODS

Ribosome preparation

Cell extract from *E. coli* A19 (in 20 mM Tris–HCl (pH 7.5), 150 mM NH_4Cl, 10 mM $Mg(OAc)_2$ and 0.5 mM EDTA) was centrifuged at 20 000 rpm using a Hitachi P65A rotor for 30 min at 4°C, and the supernatant was centrifuged at 80 000 rpm with Hitachi RP80AT rotor for 30 min at 4°C. The pellet was washed with 10 mM Tris–HCl (pH 7.6), 10 mM $MgCl_2$, 1 M NH_4Cl, 1 mM dithiothreitol, resuspended in 10 mM Tris–HCl (pH 7.6), 10 mM $MgCl_2$, 60 mM NH_4Cl, 1 mM dithiothreitol and 10 μg/ml 4-(2-aminoethyl)benzenesulfonyl fluoride, and was centrifuged through the same buffer solution containing 20% sucrose at 80 000 rpm using a Hitachi RT80AT rotor for 30 min at 4°C. The resulting fraction was washed twice with 10 mM Tris–HCl (pH 7.6), 10 mM $MgCl_2$, 1 M NH_4Cl and 1 mM dithiothreitol, and was stored at –80°C as the ribosome fraction. Subsequently, this ribosome fraction was separated into 70S ribosomes and 50S or 30S subunits by centrifugation at 25 000 rpm with a Hitachi P28S rotor for 8 hours at 4°C on 5–20% sucrose density gradients containing 10 mM Tris–HCl (pH 7.6), 10 mM $MgCl_2$, 60 mM NH_4Cl and 1 mM dithiothreitol. 70S ribosomes and subunits were concentrated by further centrifugation at 80 000 rpm with a Hitachi RP80AT rotor for 90 min at 4°C and stored at –80°C in Tris–HCl (pH 7.6), 10mM $MgCl_2$, 60 mM NH_4Cl, 1 mM dithiothreitol and 10% glycerol.

Preparation of RsgA

RsgA and the Cys mutants, with an His6-tag sequence at the N-terminal, were overexpressed in *E. coli* strain BL21(DE3) harboring a pGEMEX2 derivative containing the gene for *E. coli* RsgA under the T7 promoter sequence. The overexpression was induced by the addition of 1 mM isopropyl-1-thio-β-D-galactopyranoside. The protein was purified by chromatography using first DEAE–cellulose (Tosoh) and then Ni-IMAC Profinity (Bio-Rad), and subsequently stored at –80°C in 20 mM HEPES (pH 7.6), 10 mM $MgCl_2$, 200 mM KCl, 1 mM EDTA and 10% glycerol.

GTPase activity

The GTPase reaction proceeded at 37°C in 50 μl reaction mixtures containing 50 mM MOPS (pH 8.0), 10 mM NaCl, 10 mM $MgCl_2$, 10% glycerol, 600 nM RsgA, 100 nM 30S subunits and 100 μM GTP. A 10 μl aliquot was withdrawn from the mixture at 0, 10, 30 and 60 min and the reaction was stopped by adding 40 μl of 100 mM EDTA. The level of GTP hydrolysis was quantified by measuring the level of released phosphates using *BIOMOL GREEN*™ reagent (BIOMOL).

Conjugation of Fe(II)-BABE to RsgA

1.5 nmol of each RsgA derivative was incubated with 20 nmol Fe(II)-BABE in 100 μl solution containing 50 mM MOPS (pH 8.2), 10 mM NaCl, 1 mM EDTA and 5% glycerol at 37°C for 1 h. Free Fe(II)-BABE was excluded by gel filtration.

Formation of the 30S–RsgA complex for directed hydroxyl radical probing

Fe(II)-tethered RsgA (150 pmol) was preincubated with 2 mM GDPNP or 3 mM GDP for 15 min at 37°C. The 30S subunit (15 pmol) was incubated with Fe(II)-tethered RsgA–GDPNP (75 pmol) or RsgA/GDP (150 pmol) in 25 μl of 50 mM MOPS (pH 8.0), 10 mM NaCl, 0.1 mM EDTA, 10 mM $MgCl_2$ and 10% glycerol at 37°C for 30 min.

Directed hydroxyl radical probing

25 μl of the complex of the 30S subunit and Fe(II)-tethered RsgA was probed by initiating hydroxyl radical formation with 3 μl of 250 mM ascorbic acid and 3 μl of 1.25% H_2O_2. The reaction mixtures were incubated on ice for 10 min and quenched with 100 mM thiourea. 16S rRNA was prepared by phenol extraction and ethanol precipitation (28). Reverse transcriptase reaction was carried out in a 12-μl reaction mixture containing 50 mM Tris–HCl (pH 8.3), 75 mM KCl, 3 mM $MgCl_2$, 10 mM dithiothreitol, 0.5 mM each of dNTP, 1 pmol of rRNA, 2 pmol of 5' Texas Red labeled DNA primer complementary to a portion of the rRNA sequence, three units of ribonuclease inhibitor from human placenta (Takara) and 18 units of reverse transcriptase from Molony Murine Leukemia Virus (RNase H^-, Takara). After the addition of 3 μl of a stop solution containing 7 M

urea and 0.5% bromophenol blue, the positions of cleavages were analyzed using a fluorescence DNA sequencer (Hitachi SQ-5500).

Complex preparation for cryo-EM

To isolate the 30S–RsgA complex with high occupancy we co-incubated RsgA with 70S ribosomes; alone these ribosomes are stable as 70S ribosomes in a sucrose gradient made in buffer containing 10 mM at a Mg^{2+}. If the 70S ribosomes are co-incubated with RsgA the 70S ribosome dissociates into subunits due to the action of RsgA (14,37) and the resulting 30S subunit bound by RsgA (further stabilized by the use a non-hydrolysable GTPase analogue (GDPNP)) can be easily separated by sucrose gradient centrifugation. Accordingly, RsgA was bound to 70S *E. coli* ribosomes in the presence of GDPNP in a reaction containing 13.1 μM 70S ribosomes, 37.8 μM RsgA, 1 mM GDPNP, 37.5 mM Tris–HCl (pH 7.6), 15 mM $MgCl_2$, 100 mM NH_4Cl, 28 mM KCl and 6 mM 2-mercaptoethanol. After a 10 min-incubation at 37°C, the reaction (6 ml) was dialyzed against a 1.5 l of basal buffer containing 10 mM HEPES–KOH (pH 7.8), 10 mM $MgCl_2$, 60 mM NH_4Cl, and 6 mM 2-mercaptoethanol. The reaction was diluted by an equal volume of the basal buffer containing 5% sucrose, and loaded onto a 5–40% sucrose gradient and centrifuged at 23 000 rpm, 4°C for 17 h by Zonal rotor Ti-15. The fractions containing the 30S subunits were then sediment by centrifugation (Type 45 Ti rotor) at 39 000 rpm, 4°C for 22 h. The resulting 30S subunit pellets were re-suspended and dialyzed against the basal buffer to a concentration of 220 A_{260}/ml and stored at –80°C until use. SDS-PAGE analysis confirmed that RsgA was bound to the 30S subunits.

Electron microscopy

The 30S–RsgA complex purified by sucrose density gradient centrifugation was diluted in basal buffer and subsequently plunge frozen in liquid ethane on glow-discharged Quantifoil R2/1 grids using a Vitrobot (FEI) set to 4°C and 100% humidity with a 30 s incubation and 3–3.5 s blot time. Automated data acquisition (EPU software, FEI) was performed at eBIC (Diamond Light Source, UK) with a Titan Krios microscope (FEI) at 300 kV equipped with an energy filter (zero loss) and Falcon II direct detector (FEI). Seventeen movie frames were acquired from a 1.5 s total exposure at a calibrated magnification of 59 000× (yielding a pixel size of 1.39 Å). Dose rates of 20 electrons/Å^2/s and defocus ranges from 1.5 to 3.0 μm were used.

Image processing and structure determination

Whole-image motion correction and contrast transfer function (CTF) estimation for each movie was performed using MotionCorr (38) and CTFFIND4 (39), respectively. A total of 878 976 projection images of 30S particles were picked using the automatic picking method in RELION (40). Initially, reference-free two-dimensional classification in RELION (40) was used to discard poorly aligning particles and the best images subsequently employed in a three-dimensional refinement in RELION using a 40 Å low-pass filtered empty 30S subunit as an initial reference. The resulting reconstruction showed obvious signs of orientation bias and was therefore subjected to reweighing using a modified version of the *reweight_particle_stack.py* script (https://github.com/leschzinerlab/Relion, Michael A. Cianfrocco) to randomly remove particles from the most populated orientations. The remaining 191 440 particles were refined (without masking) and subsequently classified with RELION into six groups. After classification, refinement and particle polishing were continued with RELION for each group independently. For the refinement of the individual groups, particles were initially refined without a mask until convergence. A mask specific to the overall particle was then generated by low-pass filtering the converged volume to 15 Å, and then using an initial threshold sufficient to encompass the entire volume, a soft mask was generated. The refinement was continued using this soft mask until convergence generating the 6 volumes seen in Supplementary Figure S1 including the RsgA-AI (denoting RsgA assembly intermediate; group 1) used for model building and shown in the all figures, unless otherwise specified. In the case of group 1 (RsgA-AI), the converged volume was subject to a second classification step without angular refinement and using a mask around the ribosome head to generate three groups. The resulting volumes from the two largest groups were again subjected to the refinement and masking protocol described above, generating the RsgA-AI$_{-S3}$ and RsgA-AI$_{+S3}$ maps (Supplementary Figure S1). It should be noted that our 3D classification/refinement process revealed other volumes that show increased disorder in the 30S head and decoding site (top of h44; Supplementary Figure S1), as well as weaker or more disordered density for RsgA. We attribute these maps to complexes where RsgA is bound to the 30S subunit but either prematurely dissociates due to strong dilution during sample preparation or is bound in a less stable or dynamic conformation. Further work is required to address these dynamic 30S–RsgA-states, which may represent the initial encounter or accommodation complexes hypothesized above.

Model building, refinement and validation

A homology model of *E. coli* RsgA (sequence P39286), using *Salmonella typhimurium* RsgA (PDBID 2RCN) as a template, was built into density corresponding to RsgA (isolated from the RsgA-AI map) using Rosetta (41). The resulting model was merged with a model corresponding to the *E. coli* 30S subunit (PDB ID: 4YBB; (42)). The resulting *E. coli* 30S–RsgA refined using a jelly-body refinement in Refmac v5.8 with external restraints derived from ProSMART and LIBG (43) into the RsgA-AI map. Poorly fitting elements like the switch-1 and switch-2 regions were manually rebuilt into the density using Coot (44) and finally subjected to a local refinement using *Phenix_real_space_refine* (45,46). Ribosomal proteins were left unmodeled when they lacked corresponding density in the map when set at a threshold where the remaining ribosomal elements where generously accommodated.

Quantification and structure analysis

Reported global resolutions are based on the gold-standard FSC = 0.143 criterion (47) as determined in RELION while

local resolution was estimated with RESMAP (48) using default parameters. Presented maps are corrected according to the detectors MTF, sharpened with negative B factors initially estimated using automated procedures (49) and low-pass filtered to the estimated local resolution.

The 30S head rotation was measured using the Euler–Rodrigues formula implemented as a PyMOL plugin (http://rna.ucsc.edu/rnacenter/erodaxis.py; (50)). RsgA domain rotation was estimated using the *angle_between_domains* PyMOL plugin (https://pymolwiki.org/index.php/Angle_between_domains).

RESULTS

Structure determination and overview

RsgA was bound to the 30S subunit as it shows significantly higher GTPase activity (14) and higher affinity for mature subunits rather than immature subunits isolated from Δ*rsgA*Δ*rbfA*, Δ*rsgA* and Δ*rimM E. coli* null strains that accumulate ribosomal assembly intermediates (21,22). This was done by utilizing the ability of RsgA–GDPNP to dissociate 70S ribosomes into a 50S and a RsgA-bound 30S subunit, which can be purified by sucrose gradient fractionation (14), to prepare a highly-occupied *E. coli* 30S–RsgA complex for study by cryo-EM (see Materials and Methods). With data collected from this sample, we used 2D and 3D classification routines to select particles with well-defined density for RsgA and generated a reconstruction at an overall resolution of 5.2 Å (RsgA-AI; RsgA-Assembly Intermediate; Supplementary Figure S1), showing RsgA bound to the 30S subunit with the highest local resolution in the core of the 30S body and lower local resolution at the periphery and within the 30S head (Figure 1A–F; Supplementary Movies S1 and S2). Local resolution in the cryo-EM density corresponding to RsgA ranges largely within 4.5–5.5 Å, and therefore we built a backbone model (residues 18–346) of *E. coli* RsgA using the homologous *Salmonella typhimurium* RsgA crystal structure (94% identity; PDB ID: 2RCN) as the starting point (Figure 1F and G; see Materials and Methods). Importantly, the cryo-EM map resolved and allowed us to model residues in the switch 1 region which are often disordered and consequently absent in X-ray structures of TRAFAC-GTPases including the RsgA-GDP structure we used as a starting model.

In the RsgA-AI map, RsgA–GDPNP is bound to the subunit interface of the 30S subunit where the OB and CP-GTPase domains of RsgA interact with the 30S body, while the Zn-domain contacts the 30S head (Figure 1A and B). This orientation contrasts the binding mode of RsgA proposed in a previous cryo-EM study where RsgA is rotated roughly 180° on the surface of the 30S subunit such that the OB-domain contacts the 30S head and the Zn-domain is positioned on helix 44 (h44; Supplementary Figure S5; (33)). The binding mode observed here does mirror the overall orientation seen in a second cryo-EM reconstruction from Guo *et al*. (Supplementary Figure S5), although the improved resolution of the RsgA-AI map affords a detailed understanding of the interaction surface and mechanism by which the GTPase pocket is activated (discussed below). Additionally, the RsgA-AI map indicates that although initially bound to a mature 30S subunit, RsgA induces conformational changes in the 30S subunit that destabilize r-proteins uS2, uS3, uS7, uS12 and bS21 such that they are significantly underrepresented in the RsgA-AI map. This profound underrepresentation of r-proteins was not observed in the previous reconstruction of the 30S–RsgA complex (23) and may be attributable to improvements in cryo-EM methodology (51) or to the purification of the sample via a sucrose gradient before cryo-EM analysis which yields a more homogenous 30S–RsgA sample. In the RsgA-AI map, h44 is stably docked in its canonical position as seen in a mature 30S subunit which is in line with the idea that RsgA binding is associated with h44 assuming its mature conformation during the last stages of ribosome assembly (7,23,24). Finally, the 30S head is rotated ∼12° around an axis that is roughly perpendicular to the axis characteristic of 30S head rotation seen in the 70S (50) and its movement can be described as a nodding rather than a rotation (Supplementary Figure S2A). Although unusual, a similar nodding of the 30S head was recently described in the structures of the 30S initiation complexes (52) (Supplementary Figure S2B).

Tertiary binding proteins are underrepresented in the RsgA-AI cryo-EM map

Typically, the Group IV and V particles associated with the late stages of 30S assembly are deficient in r-proteins uS2, uS3 and bS21 to varying extents (7). These proteins as well as uS7, uS12, are strongly underrepresented in the RsgA-AI map when the threshold is set close to the level of the solvent that generously accommodates the rest of the subunit (Figure 1H and I). Even if the map is low pass filtered (i.e. to 12 Å) to accentuate disordered elements in the density, the bulk of uS2, uS3, uS12 and bS21 remain the weakest elements in the map (Supplementary Figure S6). The weakness or underrepresentation of r-proteins in the cryo-EM map can stem from either substoichiometric binding and/or local disorder in the r-proteins indicating that they are bound in a dynamic fashion; two possibilities that cannot be distinguished in the cryo-EM map. Secondary structure elements of r-proteins uS10 and uS14 that are in proximity of the uS3 binding site show weak, fragmented density at high thresholds but the density becomes more evident as the threshold is lowered (Supplementary Figure S6). This suggests that there is local disorder in these proteins resulting from the lost interactions with uS3, which as mentioned, is completely absent in the map.

Among the underrepresented proteins, uS12 is the closest to the RsgA binding site and its underrepresentation can be rationalized by a direct steric clash between the loop of uS12 (residues 39–49) that is deeply inserted between h18 and h44 and the N-terminal extension (NTE) of RsgA. Ribosomal proteins uS2, uS3 and bS21 are more remote from RsgA and accordingly RsgA-induced conformational changes in the 30S subunit structure must lead to their destabilization. To address the structural variability in the 30S head, we employed a focused 3D classification/refinement routine to separate the dataset into two populations with an overall resolution of 5.4 and 5.8 Å, respectively (Supplementary Figure S1, volumes RsgA-AI$_{-S3}$ and RsgA-AI$_{+S3}$). These two volumes differ most obviously in the orientation

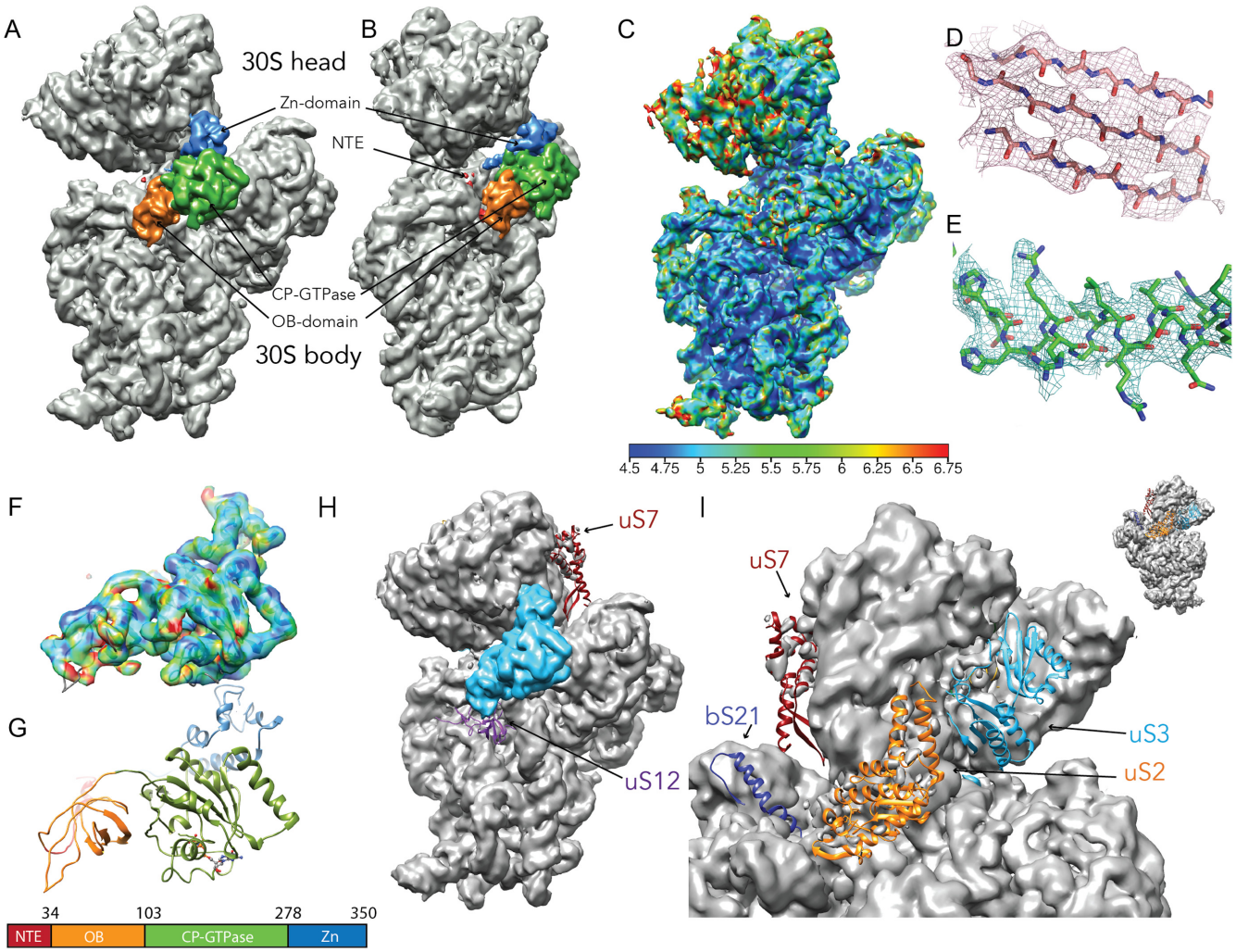

Figure 1. Overview of 30S–RsgA–GDPNP structure. (A and B) The overall structure of the 30S–RsgA–GDPNP complex is shown with density corresponding to the 30S subunit (gray) and the RsgA OB-domain (orange), CP-GTPase domain (green) and Zn-domain (blue) colored distinctly. Fragmented density corresponding to the NTE of RsgA is shown in red. The map is low-pass filtered to the overall resolution of 5.2 Å and shown from the subunit interface (**A**) and A-site side (**B**). See Supplementary Movie S1 for additional views. (**C**) The local resolution of the 30S–RsgA–GDPNP structure as determined by ResMap is projected onto the cryo-EM map (5.2 Å) and colored per the key in the panel. See Supplementary Movie S2 for additional views. (**D** and **E**) The cryo-EM maps filtered to the local resolution (4.5 Å) around r-proteins uS5 and uS15 are consistent with resolution estimates. Namely in panel E the density begins to separate according to the β-strands and in panel D bulkier side chains become visible. (**F**) Local resolution is projected onto the isolated density corresponding to RsgA, colored per the key in panel C and low pass filtered to the overall resolution of 5.2 Å. (**G**) Model of RsgA highlighting the different domains of the protein. Domain boundaries and secondary structure designations are based on Shin *et al.* (29). (**H** and **I**) The 30S–RsgA–GDPNP cryo-EM map is rendered at a low threshold to highlight r-proteins that are most significantly unaccounted for by the density. In panel H the map is shown from the subunit interface with RsgA colored blue and in panel I the map is shown from the solvent side (see inset) with a focus on the 30S head region. In Supplementary Figure S6, the maps are rendered at additional thresholds and with a low pass filter applied to further illustrate the underrepresentation of the r-proteins in the map.

of the 30S head (Supplementary Figure S2C) and the relative strengths of density corresponding to ribosomal protein uS3 (Figure 2A and B). Specifically, density corresponding to uS3 is significantly weaker in the map designated RsgA-AI$_{-S3}$. As seen in Figure 2C–E where individual 16S rRNA residues are colored according to their relative displacement, when models corresponding to the two maps are compared (i.e. RsgA-AI$_{-S3}$ versus RsgA-AI$_{+S3}$), it can be seen that 16S rRNA residues surrounding the uS3 binding site undergo a significant conformational change; specifically, in the RsgA-AI$_{-S3}$ map the 16S rRNA has a more open structure with the backbone of h34 shifting by ∼7 Å. The observed displacement of the rRNA residues is most significant around the irregular backbone structure of h34, which forms part of the uS3 binding site (Figure 2C–E). Although the open conformation can be both the cause and effect of the observed underrepresentation of r-proteins, the change in h34 could disrupt the uS3 binding site and prevent the C-terminal β-sheet of uS3 from packing against the minor groove of h34 as seen in the structure of the mature 30S subunit.

RsgA-induced conformational changes in the 30S head may destabilize or slow incorporation of the tertiary r-proteins to promote a favorable maturation pathway, in-line

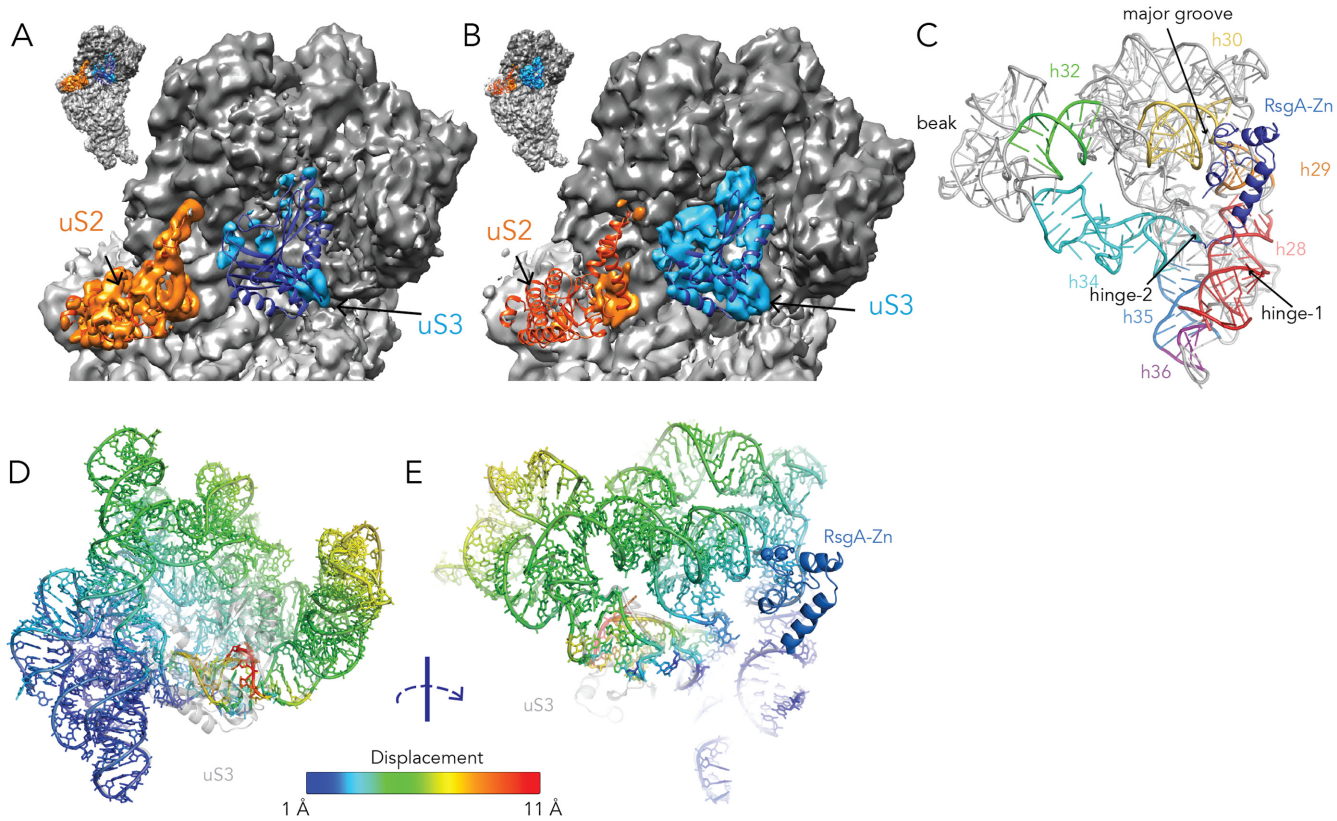

Figure 2. Classification of the 30S–RsgA dataset results in two 30S subunit conformations. (**A** and **B**) The two reconstructions that result from the 3D classification procedure, namely an RsgA Assembly Intermediate without uS3 (RsgA-AI$_{-S3}$) and an RsgA Assembly Intermediate with uS3 (RsgA-AI$_{+S3}$) are shown. The density corresponding to uS3 becomes stronger after classification, although it is still weaker than the surrounding proteins. Here, the density corresponding to the 30S head (dark gray) and body (light gray) are colored distinctly. Additionally, density corresponding to the r-proteins uS2 (orange) and uS3 (blue) have been isolated using a mask generated from an aligned 30S subunit structure (PDBID 4ybb). These isolated densities are set at an equivalent threshold such that they have the same strength as seen in the originating map. (**C**) To highlight helices discussed in the text, the 16S rRNA component of the 30S head is shown in the same orientation as panel E with selected 16S helices colored distinctly. The Zn-domain of RsgA is shown as a blue ribbon to indicate the position relative to the highlighted helices. (**D** and **E**) The 16S rRNA component of the 30S head corresponding to the RsgA-AI$_{-S3}$ (colored) and RsgA-AI$_{+S3}$ (gray) have been aligned and colored according to the key to illustrate the displacement (in Å) of corresponding residues in the two structures. The structures are shown from the solvent side (D) and subunit interface side (E). uS3 is shown as a transparent grey ribbon to illustrate its binding site on h34. The Zn-domain of RsgA is shown as a blue ribbon (panels C and E) to indicate its position relative to residues that experience increased displacement.

with the notion that assembly factors act by delaying specific folding steps to avoid kinetic traps (10). In this respect, previous work from Mulder and colleagues demonstrates that premature binding of tertiary proteins to the 3′ domain, in particular rapid binding of uS2 prior to uS3, results in kinetically trapped assembly intermediates that convert slowly to mature 30S subunits (6).

RsgA is positioned to monitor key features of the 30S mRNA/tRNA binding sites

The overall positioning of RsgA on the 30S subunit (Figure 3) indicates that RsgA monitors residues that play key roles in mRNA decoding at the A- and P-tRNA binding sites. For example, in the A-site the OB-domain of RsgA is positioned between h18 and h44, with the loop connecting β1 and β2 of RsgA (Phe48- His51; Figure 3A, Supplementary Figure S3A) inserted into the minor groove of h44 near A1410 and the bulged A1492/A1493 which are essential for monitoring correct mRNA decoding in the 30S A-site (30). The displacement of A1492-93 from h44 is consistent with chemical probing experiments showing that the reactivity of their base-paring partner, A1408, increases in the presence of RsgA–GDPNP (53). Overall the binding mode of RsgA with h44 is similar to that of initiation factor IF1 in that both factors bind to overlapping sites on h44 and displace A1492 and A1493 from the helical stack into a pocket formed by the OB domain (Supplementary Figure S3B). In the case of IF1, its interaction with h44 serves as anchoring point for the other two initiation factors (IF2 and IF3) during the initiation phase of protein synthesis (52,54), suggesting that the OB domain of RsgA may similarly act as anchoring point for its remaining two domains.

Preceding the OB domain, there is a weakly conserved N-terminal extension (NTE, residues 1–33 in *E. coli*, Supplementary Figure S4, red bar) of variable length, which is generally longest in gammaproteobacteria including *E. coli* (28). By low pass filtering the cryo-EM map, density corresponding to the unstructured NTE (Figure 1A and B, red density) can be observed as continuous den-

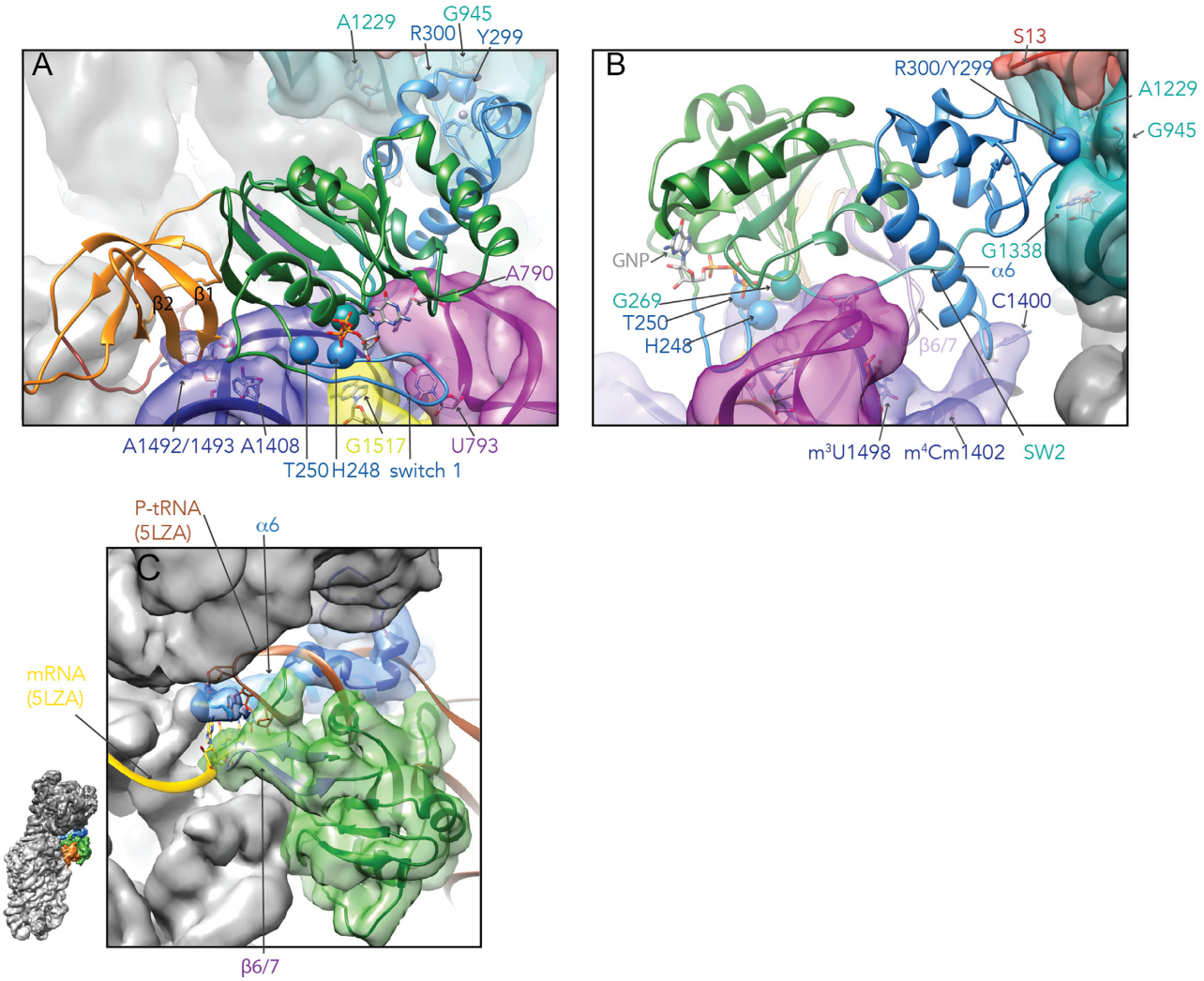

Figure 3. RsgA binds to the 30S mRNA/tRNA binding sites. The RsgA binding site is shown from the subunit interface (**A**) and E-site side (**B**) to highlight sites of potential interaction important for RsgA function. RsgA is shown in a ribbon representation with the domains colored as in Figure 1G. Residues of switch 1, switch 2 and the β6/7 hairpin are colored marine blue, deep teal and light purple, respectively. The backbone CA atom of selected residues are rendered as spheres. Cryo-EM density (5.2 Å lowpass filter, –100 *B*-factor) has been segmented and colored according to the underlying 30S subunit elements (purple, h44; yellow, h45; magenta, h24; cyan, h29/30; red, S13; gray, all else). The density corresponding to RsgA has been omitted for clarity but can be seen in Supplementary Figure S3. (**C**) The mRNA (yellow ribbon/sticks) and P-tRNA (brown ribbon/sticks) from a 70S-fMet-tRNAfmet cryo-EM structure (PDBID 5LZA) have been superimposed on the 30S–RsgA structure to illustrate how the β6/7 hairpin and C-terminal α-helix (α6) of RsgA enter the 30S P-tRNA site. Density corresponding to h18 is not shown to facilitate visualization of the 30S P-tRNA binding site.

sity running from the N-terminal of the OB-domain, toward the A-tRNA decoding site where it loops up over h18 (C518/G529–G530, Supplementary Figure S3C) and finally emerging near h34 of the 30S head. This placement of the NTE is consistent with chemical probing experiments that show G530 is protected from chemical modification by RsgA–GDPNP (53).

In the 30S P-site, the CP-GTPase domain of RsgA clamps around h44 near the interface formed between the minor groove of h44, the tetraloop of h45 and the tip of h24 (Figure 3B; Supplementary Movie S3). One arm of this clamp is formed by the β-hairpin (β6 and β7 of RsgA), which approaches the major groove of h44 near the modified m^3U1498 (Figure 3B and Supplementary Figure S3D). This residue, besides being one of the rRNA residues modified in the *E. coli* 16S rRNA, is also important for positioning the mRNA in the 30S P-site (55). The second arm of the clamp is formed by the switch 1 region (238–250) connecting α4 and β12, which approaches the minor groove of h44 near A1408 (Thr251), G1517 in the loop of h45 (His248; Figure 3A and B and Supplementary Figure S3E and F) and finally the bulged U793 in h24 (Leu245). In the 30S–RsgA model, h44 and the loop of h45 appear completely docked onto the 30S subunit in the so-called "engaged" conformation characterized by a hydrogen bond network between the minor groove of h44 and G1517–A1519 forming the loop of h45 (56–58). This is significant as the loop of h45 contains 3 modified residues, m^2G1516, $m^6{}_2$A1518 and $m^6{}_2$A1519, and its interaction with h44 is conformationally dynamic; namely the hydrogen bond network between h44 and h45

can be disrupted leading to a disengaged conformation of the loop in response to the antibiotic streptomycin, which stabilizes the near-cognate codon-anticodon interaction at the A-site, and more importantly by the lack of dimethyl modifications on A1518 and A1519 (56–58). The functional significance of the RsgA h44/45 interface is evidenced by the observation that the antibiotic streptomycin inhibits the ribosome-dependent GTPase activity of RsgA without affecting binding (14,16).

The Zn-domain forms a bridge with the head of the 30S subunit where Tyr299 approaches G1338 (h29) and Arg300 extends between the backbones of G945–A946 and A1229–C1230 (Figure 3A and B and Supplementary Figure S3G). Although remote from the mRNA decoding site these elements are involved in P-tRNA binding with G1338, specifically, participating in a universally conserved A-minor interaction with the stem of P-site bound initiator tRNA (52,59,60). The C-terminal α-helix (α6) of the Zn-domain does extend back into the mRNA channel where the P-tRNA binds, and approaches the β6/β7 hairpin of RsgA and C1400 (h44) of the 16S rRNA (Figure 3B and C) which positions the P-site codon–anticodon complex by stacking against the last base pair (52,61). Notably α6 shares a highly conserved interface (Arg325) with the CP-GTPase domain (Asp142) and approaches switch 2 (Figure 3B) which supports the observation that truncating RsgA to remove its C-terminal extension including α6 hinders the 30S-dependent GTPase activity of RsgA (24).

Conformational changes in RsgA activate the GTP binding pocket

In the current 30S–RsgA structure the GTP binding pocket is well-ordered with the switch 1 and 2 regions readily visible in the cryo-EM map. Comparing the structure of free RsgA in its GDP form (28) with the 30S-bound RsgA–GDPNP form presented here (Figure 4A) reveals that the β-hairpins formed by β6/β7 and β12/β13, together with the OB-domain, undergo a concerted movement relative to the core of the CP-GTPase domain, which can be described as transformation involving a small displacement (6.4 Å) and 22° rotation around a single axis (blue cylindrical arrow in Figure 4A). This rotation has a significant effect on β6 and β13 (Figure 4A), resulting in conformational changes that close the GTP-binding pocket around the GDPNP molecule (Figure 4B). For example, the invariant glycine residue (Gly269 in RsgA) following β13 is displaced by ∼8 Å relative to its position in the GDP structure (Figure 4B). This is significant because in GTPases residues homologous to Gly269 typically form a hydrogen bond with the γ-phosphate (27) and the observed GDPNP-dependent displacement correctly positions Gly269 to form such an interaction. In the GTPase family of proteins, conformational changes in this glycine residue, driven by the γ-phosphate interaction, influence the conformation of residues in the adjacent switch 2 region (27). Accordingly, switch 2 residues that form a short 3_{10} helix in the RsgA–GDP structure (28) unravel into an extended conformation in the RsgA–GDPNP model (Supplementary Movie 4). In this conformation switch 2 residues approach A790 at the tip of h24.

The rotation of the OB-domain further contributes to the closing of the GTP pocket through displacement of β6 (orange arrow, Figure 4B) which flanks switch 2 and can thus influence its conformation. Moreover, opposite the β6/β7 hairpin, switch 2 is buttressed by the C-terminal α6 which therefore couples the relative arrangement of the Zn domain to the GTP pocket in agreement with the previous reports that α6 is essential for RsgA´s GTPase activity (24). Interactions between RsgA and h44 (Thr251/A1408), h45 (His248/G1517) and h24 (Leu245/U793) (Figure 3A), assist in ordering the long switch 1 region, which is disordered in the RsgA-GDP structure, further closing the GTP binding pocket and moving Thr250 of the G2 motif (Figure 4B) into a position where it can interact with the γ-phosphate of GDPNP and the Mg^{2+} ion as characteristic of the GTPase family proteins. In summary, the closing of the GTP pocket is dependent on (i) the relative positions of the β6/β7 hairpin, OB- and Zn-domain, which in turn influence the G3 and the switch 2 region, and (ii) the conformation of helices 44, 45 and 24 that form an interface with the ordered switch 1 region.

As mentioned, RsgA belongs to the HAS-GTPase subfamily, and therefore, the catalytic residue in switch-2 that positions the active site water in typical GTPases (Gln61 in Ras and His85 in EF-Tu) is replaced by a hydrophobic valine residue in RsgA (Supplementary Figure S4, black star), which indicates that RsgA employs an alternative mechanism of GTP hydrolysis (31). As seen in Figure 4C, a comparison between the GTP binding pockets of EF-Tu (62) and RsgA highlights their similarities but also reveals that the backbone position of the highly conserved His248 in switch 1 of RsgA (Supplementary Figure S4, black star) allows its side chain to occupy a position that overlaps with the catalytic His85 of EF-Tu (found in switch-2). Moreover, in the 30S–RsgA model, G1517 (h45 of the 30S subunit) is placed such that it can position His248 (Figure 4C) similar to the role played by the α-sarcin loop in the activation of EF-Tu's GTPase activity. Namely in EF-Tu, GTP hydrolysis is stimulated by the correct positioning of His85 relative to the active site water via an interaction with the phosphate group of A2662 located in the α-sarcin loop of the 23S rRNA (62). Accordingly, RsgA uses a unique mechanism for GTP hydrolysis where the catalytic residue originates in switch 1 rather than from switch 2 as in prototypical GTPases, and it parallels the classical TRAFAC-GTPases like EF-Tu in that the rRNA plays the role of an activator by correctly positioning the catalytic histidine residue. This difference in the architecture of the GTP binding pocket can be exploited when designing RsgA-specific anti-microbials.

Mapping RsgA interaction sites during GTP hydrolysis using directed hydroxyl radical probing

To understand how the interaction of RsgA with the 30S subunit changes in response to GTP hydrolysis, we employed directed hydroxyl radical probing with Fe(II)-BABE. For this purpose, each mutant of RsgA is preferred to have only a single cysteine residue, whereas wild type RsgA has total five cysteine residues, the last three of which might be critical for ribosome-dependent GTPase activity due to their direct involvement in binding the zinc ion

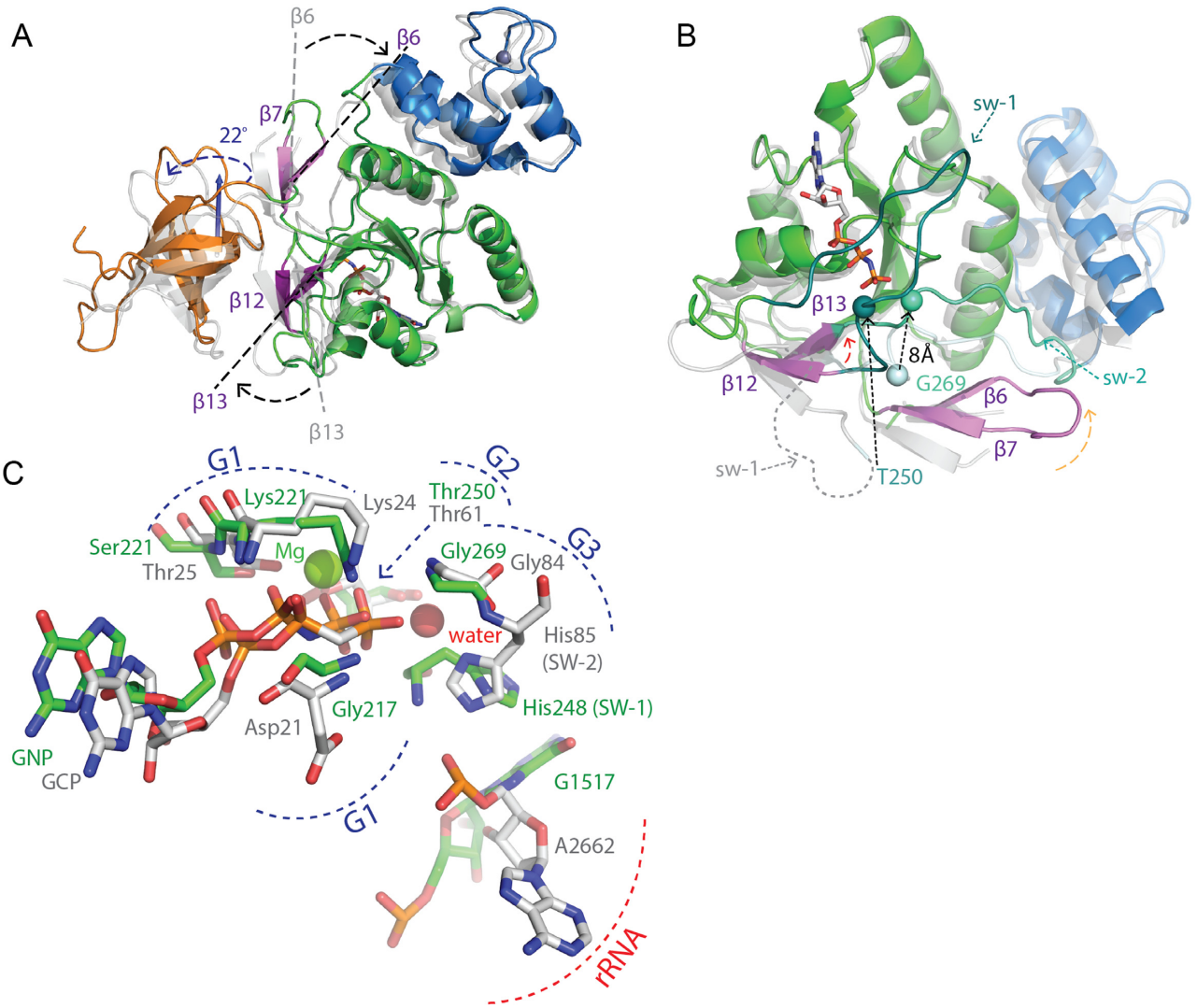

Figure 4. Activation of RsgA GTPase pocket. (**A**) Aligning the GTPase domain of the isolated RsgA–GDP (PDB ID: 2rcn) structure and the current ribosome-bound RsgA–GDPNP model indicate that the OB-domain and the two β-hairpin elements (β6/7 and β12/13) undergo a displacement of 6.4 Å with a rotation of 22° around the indicated axis (blue cylindrical arrow). (**B**) The rotation of β13 results in an ∼8 Å displacement of G269 (G3/switch-2) such that it becomes poised to interact with the γ-phosphate as typically observed in GTPases. Switch 1 and Switch 2 are abbreviated as sw-1 and sw-2, respectively. (**C**) Comparison of the GTPase pocket active site residues as seen in the EF-Tu-GDPCP X-ray structure (light gray, PDB ID: 4v5l, (62)) and the RsgA–GDPNP model (green). Key active site residues are drawn as sticks. The active site Mg^{2+} ion and water molecule are drawn as seen in the EF-Tu-GDPCP structure.

(28,29). Since these three cysteine residues were expected to be resistant to modification with Fe(II)-BABE due to its tight binding to a zinc ion, only the former two cysteine residues at positions 64 and 148 were substituted with alanine. This mutant RsgA, designated RsgA(-Cys), has a ribosome-dependent GTPase activity about half of that for wild type RsgA. Based on this background, we designed 33 RsgA mutants, each having only one exposed cysteine residue. The mutant RsgA proteins were overexpressed, and purified by anion exchange and affinity column chromatography. They were subjected to directed hydroxyl radical probing.

To mimic two different steps of RsgA binding and action on the ribosome, each RsgA variant to which Fe(II) was tethered was incubated with the 30S subunit in the presence of either GDPNP or GDP. It has been shown that RsgA·GDPNP but not RsgA·GDP stably binds to the 30S subunit at a normal salt concentration containing 100 mM ammonium chloride, while both RsgA·GDPNP and RsgA·GDP bind to the 30S subunit at a low salt concentration containing 10 mM ammonium chloride (53). In the present study, Fe(II)-tethered RsgA was mixed with the 30S ribosomal subunit in the presence of GDPNP or GDP to form a complex at a low salt concentration, and cleavages of 16S rRNA by hydroxyl radicals generated from Fe(II) were detected by primer extension. We confirmed that Fe(II) tethered to RsgA(-Cys), as well as to wild type RsgA, yields no detectable 16S rRNA cleavages in the presence of GDPNP or GDP. Cleavage signals were identified from 17 of the 33 variants in the presence of GDPNP or GDP

(Figure 5); these included nine variants in the OB-domain, two variants in the GTPase domain and six variants in the Zn-binding domain (Figure 5A). We confirmed that these 17 variants retained a ribosome-dependent GTPase activity (Supplementary Figure S7). No signals were detected when we used the remaining variants each having a mutation at residues 48, 57, 80, 121, 152, 171, 194, 202, 204, 226, 294, 298, 309, 322, 324 or 331 (*E. coli* numbering).

Overall, the sites of cleavage originating from the individual domains of RsgA correspond well with the domain placement observed by cryo-EM (Figure 5C and D). In the presence of GDPNP, cleavages occurred from nine OB-domain variants: they cleaved 16S rRNA predominantly around the A-site, in particular, within h18 and h44 of the 30S body, and within h34 of the 30S head (Figure 5C; orange spheres). In comparison, CP-GTPase domain variants cleaved 16S rRNA regions towards the P-site including residues in h24, h28 and h30 (Figure 5C; green spheres). Finally, the sites of cleavage from the six variants in the Zn-domain were distributed around the P-site and E-site: variants closest to the Zn binding motif cleaved predominantly in the 30S head (i.e. helices 29, 30 and 34) while those originating from the C-terminal helix (α6) where more distributed in both the head and platform (helices 24, 28, 29, 30, 34 and 44) (Figure 5C; blue spheres). When GDPNP was substituted by GDP, the region of cleavage in the 30S subunit from each domain of RsgA did not alter significantly; namely the region of contact with each RsgA domain is unchanged after GTP hydrolysis (Supplementary Table S1, Figure 5C and D). However, the pattern of cleavages originating from the individual domains in the presence of GDP is different from that in the presence of GDPNP. For example, 25% of cleavage sites from the OB-domain variants increased in intensity, while only 38% showed lower intensity. By contrast, variants in the CP-GTPase domain and Zn-domain did not show any increased cleavage intensity, while 66% and 90% of the associated cleavage sites showed decreased intensity, respectively (Supplementary Table S1). Likewise, when Figure 5C and D are compared, it is evident that the number of strong cleavage sites from the CP-GTPase domain and Zn-domain variants (+++ in the OB- or CP-GTPase domain and ++ in the Zn-domain) are markedly reduced in the presence of GDP. These results indicate that in the GDP form of RsgA, the predominant interaction interface for RsgA is the OB domain, which remains closely associated with the ribosome, while in the GTP form, all three domains are similarly associated with the 30S subunit. Reduction in the number of cleavages in the GDP form of RsgA might reflect lower affinity of the GDP form of RsgA with the 30S subunit than that of the GDPNP form (53). Furthermore, as seen in Figure 5C cleavage sites in the 30S head are more widely dispersed than those in the 30S body which is consistent with conformational changes observed in h30/h32/h34 (Figure 2C and D).

DISCUSSION

Taken together, the single particle cryo-EM and directed hydroxyl radical probing experiments provide insight into the molecular mechanisms underlying the ability of RsgA to interact with and sense the state of the 30S subunit to guide its maturation. First, the RsgA-AI maps indicate that in the 30S–RsgA structure the 16S rRNA forming the 30S head has a more open conformation and the binding of tertiary r-proteins uS2, uS3, uS12 and bS21 is destabilized (Figure 2). Second, the RsgA-AI structure reveals that the main points of interaction between RsgA and the 30S subunit are mediated by ribosomal elements that are also involved in binding and decoding of the mRNA/tRNA (Figure 3). Importantly, these contact sites often involve or are dependent on rRNA residues that are modified (methylated) during the 30S maturation process and their modification generally contributes to fine-tuning ribosome structure and function often by stabilizing interactions in the P site (55). Moreover, the directed hydroxyl radical probing experiments reveal that in the GDP form the OB-domain is the dominant interface for 30S contact, while in the GTP form all three domains are involved in 30S binding (Figure 5). Finally, the RsgA-AI structure reveals that RsgA uses a structural variation of the prototypical GTP binding pocket where the catalytic residue originates from switch 1 rather than from switch 2. Moreover, the 16S rRNA of the maturing 30S subunit plays an activating role in the GTPase activity of RsgA by influencing the ordering of switch 1 and directly positioning the catalytic residue. This shows that the 16S rRNA can function in GTPase activation like the 23S rRNA of the 50S subunit does with other TRAFAC-GTPases like EF-Tu (Figure 4) (30).

Prior work has established that RsgA integrates into the 30S assembly pathway after the action of RbfA, a 30S assembly factor that facilitates correct folding of the central pseudoknot region (10), where RsgA actively promotes the release of RbfA from the 30S subunit (21,24). Cryo-EM studies indicate that, similar to the RsgA-30S structure presented here, uS12 and uS3 are underrepresented in the 30S–RbfA complex (23), and additionally h44 is pulled out of its canonical binding site (11), which is significant as h44/h45/h24 serves as a large interaction surface for RsgA (Figure 3). Our directed hydroxyl radical probing experiments indicate that the OB-domain of RsgA can interact with the 30S subunit independent of the CP-GTPase and Zn-domain (Figure 5). Accordingly, during the initial encounter of RsgA with the 30S subunit, the OB-domain may act as an anchoring point to tether RsgA to the undocked h44, and in turn to the 30S subunit. Moreover, the N-terminal extension of RsgA, which inserts between h44 and h18 (Supplementary Figure S3C), may substitute for the missing uS12 and facilitate h44 docking into its canonical site. The importance of the OB domain for mediating initial contact with the assembling 30S subunit is supported by the work of Jeganathan and colleagues showing that efficient RsgA binding to immature subunits is dependent on the OB-domain (24). As mentioned, RsgA, specifically the C-terminal extension, triggers the release of RbfA from the 30S subunit (21,24). The earlier cryo-EM structure of the RbfA–30S complex indicates that RbfA displaces h44 from its canonical position (11), while the present cryo-EM structure of the 30S–RsgA complex indicates that RsgA promotes h44 docking by clamping around the h44/h45/h24 interface to stabilize the docked h44 conformation. Accordingly, the RsgA-induced conformational changes in h44 may weaken RfbA-30S interactions to facilitate its release.

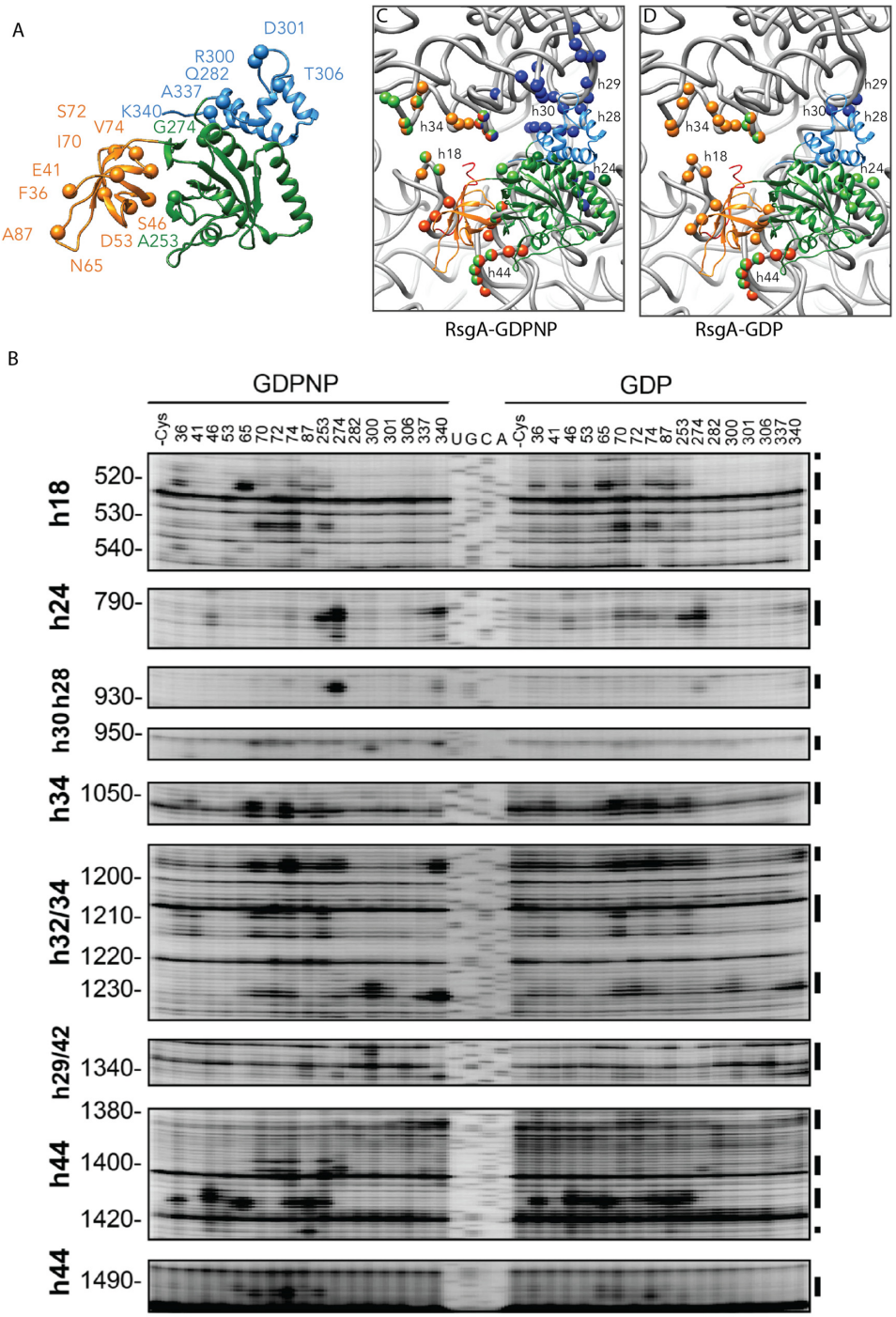

Figure 5. Directed hydroxyl radical probing of the 30S subunit upon binding of RsgA in the presence of GDPNP or GDP (**A**) The position of the 17 Cys mutants (CA atoms drawn as spheres) used for tethering Fe(II) to RsgA are highlighted on the structure of RsgA–GDPNP. As seen in Supplementary Figure S7 the 17 Cys mutants also show detectible 30S-dependent GTPase activity indicating that the mutation does not significantly hinder interaction with the subunit. Individual domains are colored as in Figure 1G. (**B**) Sites of cleavage in the 16S rRNA by hydroxyl radicals from Fe(II) tethered to each RsgA variant were detected by primer extension. The 30S subunit was probed with a bound RsgA variant in the presence of GDPNP or GDP (left and right lanes, respectively). The lanes with the -Cys label indicate the parental RsgA variant containing no cysteine residues other than those in the C-terminal domain that are involved in zinc binding. The numbered lanes correspond to the residue number at which an additional cysteine residue is introduced into the -Cys variant. The sequencing lanes (middle) with the same primer are designated by U, G, C and A. The positions of selected 16S rRNA nucleotides, together with their associated helices, are shown on the left, while bands of interest are marked by bars on the right. (**C** and **D**) The cleavage sites detected by the directed hydroxyl radical probing of the RsgA–GDPNP–30S complex (C) or the RsgA–GDP–30S complex (D) are mapped on a model of the 30S subunit. The sites of cleavage are highlighted by rendering the corresponding backbone phosphate atom as a sphere and coloring the sphere according to the domain in which the Fe(II) is tethered. The domain coloring scheme is as illustrated in panel A where additionally dark orange and green are used to indicate cleavage sites designated with an +++ intensity in Supplementary Table S1 and lighter orange, green and blue indicate sites designated with ++ intensities. Spheres that have two colors are cleaved by variants in multiple domains.

Underrepresentation of uS12 in both the RbfA (11,23) and RsgA complexes indicates that these factors work together to delay stable incorporation of uS12 until the very late stages of 30S maturation. uS12 is adjacent to both h44 and the central pseudoknot and its absence may allow flexibility in these elements as required during the earlier stages of 30S maturation; for example, access of the rRNA modification enzymes (i.e. the methyltransferases like RsmA(KsgA)) to their target residues which predominantly lie within the 30S mRNA/tRNA decoding channel (55). It is important to point that Sashital and colleagues observe a relatively high abundance of uS12 in late stage intermediates purified from wild type cells (7). In this regard, it is most likely that uS12 underrepresentation in the RsgA-AI map reflects that uS12 is dynamically bound in the presence of RsgA–GDPNP such that it is tethered to the 30S subunit by its long N-terminal extension that reaches into the core of the 30S subunit but not stably accommodated in its canonical binding site. In fact, density corresponding to the short N-terminal helix is evident in the RsgA-AI$_{-S3}$ and RsgA-AI$_{+S3}$maps.

Concerning the underrepresentation of uS2, uS3 and bS21 in the 30S–RsgA–GDPNP complex, it is important to note that they represent the slowest binding tertiary proteins in both, *in vitro* assembly reactions, and when 30S assembly intermediates are purified from wild type cells (5,7). Furthermore, assembly intermediates purified from strains specifically depleted in RsgA (Δ*rsgA*) show a low abundance of uS2, uS3 and bS21 (17,22). In general, particles purified from these depleted strains are presumed to be intermediates of low free energy that are slow to convert into mature ribosomes, and RsgA destabilizes their structure to guide them onto a kinetically favorable assembly pathway (17). The RsgA-AI maps show structural evidence of this destabilization, indicating that RsgA–GDPNP can significantly alter the structure of h34 around the uS3 binding site (Figure 2). It should be noted that the cryo-EM experiments cannot distinguish if the r-proteins are underrepresented because they are depleted from the sample or display local disorder that weakens their corresponding density. To drive 30S maturation, after destabilizing the subunit structure, RsgA should direct it towards a favorable assembly pathway. This direction could be evidenced by the two RsgA-AI$_{-S3}$ and RsgA-AI$_{+S3}$ maps (Figure 2), such that the RsgA-AI$_{-S3}$ map, with the altered h34, represents a destabilized intermediate state and the RsgA-AI$_{+S3}$ map represents a subsequent state where the 30S head is refolding with h34 and uS3 in a canonical state. This interpretation is in line with the work of Mulder and colleagues indicating that binding of uS3 prior to uS2 avoids formation of kinetically trapped assembly intermediates that convert slowly to mature 30S subunits (6).

Recently, connections have been drawn between 30S maturation and 30S initiation and it has been suggested that the maturation of the small ribosomal subunit involves a 'test drive' consisting of an initial round of initiation that yields a 70S initiation complex on which the rRNA undergoes the final processing steps (17,63). In this light, it is important to point out that there are substantial parallels between the 30S–RsgA complex presented here and 30S initiation complexes (52,54). This includes, for example, the similarity in the 30S head rotation (Supplementary Figure S2C) and in the binding position of IF1 and the OB-domain described above (Supplementary Figure S3B). At the structural level, there are parallels between the interface formed by either switch 1 of RsgA, or the C-terminal domain of IF3, and helices 44, 45 and 24 of the 16S rRNA (52,54). Moreover, RsgA approaches C1400 and U1498, which are important for positioning the codon-anticodon complex in the initiation complex (Figure 3C and Supplementary Figure S3D; (52,55)), and G1338 (Supplementary Figure S3G), which makes a universally conserved contact with the stem of the initiator tRNA and has been implicated as being critical for triggering rRNA processing in the 'test drive' round of initiation (59,60,63). Accordingly, RsgA may probe the maturing 30S subunit for its ability to form initiation-like interactions before triggering its own GTPase activity, dissociating from the subunit and allowing maturation to progress to the next step, i.e. the initial initiation 'test drive'.

Activating the GTPase pocket of RsgA is driven by conformational changes in RsgA that are promoted or stabilized by interactions with the ribosome. For example, the relative arrangement of the OB- and CP-GTPase domain in the ribosome bound structure reposition β6 and β13, which in turn restructure the G3 and switch 2 motifs in the GTP pocket (Figure 4). Importantly, several modified rRNA residues lie at the center of many of the potential interaction sites with the CP-GTPase domain of RsgA. For example, the hairpin formed by β6/7 approaches m^3U1498 (Supplementary Figure S3D), while switch 1 residues interact with G1517 in the loop of h45 (Figure 3A and B, and Supplementary Figure S3F) whose conformation varies depending on the methylation state of the neighboring nucleotides, $m^6{}_2$A1518 and $m^6{}_2$A1519 (57). In this regard, if these residues in the loop of h45 are unmodified, G1517 would not be positioned to form suitable interactions with switch 1, which in turn could prevent switch 1 from ordering and forming the larger interface that clamps h44 in its canonical position. Preventing premature h44 docking would be important in the situation where docking precludes subsequent access of the modifying enzyme to its target residue. In fact, this is the case with the methyltransferase RsmA(KsgA), which requires h44 to be displaced to access and modify residues in the loop of h45 ($m^6{}_2$A1518 and $m^6{}_2$A1519; (64)). The ability of RsgA to respond to the conformation of the 30S decoding center is further supported by the observation that antibiotics targeting the 30S decoding center dramatically affect the GTPase activity of RsgA (14,16). Taken together these results provide a structural basis to rationalize RsgA´s suggested role as a checkpoint protein by indicating how RgsA probes the maturation state of the decoding center before activating its own GTPase activity and triggering its release from the ribosome. Generally, in TRAFAC-GTPases like EF-Tu, GTP hydrolysis and subsequent Pi release is associated with unraveling conformational changes in the switch-1 and -2 regions, which in turn disrupt the ribosomal interface and results in dissociation of the factor from the ribosome (30). In the case of RsgA, Pi release would also disrupt interaction between the switch regions and the γ-phosphate that contribute to the ordering of switch-1 and switch-2. As switch-1 forms a major interaction surface with the 30S subunit,

its unraveling would lead to the dissociation of RsgA from the 30S subunit and allow maturation to proceed. This is in line with the presented directed hydroxyl radical probing results suggesting that GTP hydrolysis and Pi release weaken the interaction of CP-GTPase domain and Zn-domain with the 30S subunit to reduce the affinity of RsgA with the 30S subunit, allowing its dissociation from the 30S subunit.

In conclusion, the cryo-EM and hydroxyl radical probing experiments contribute to our understanding of RsgA´s role in 30S biogenesis by providing structural evidence that RsgA destabilises the 30S head structure, including tertiary r-protein binding, to rescue kinetically trapped assembly intermediates. Moreover, they reveal the mechanism by which RsgA evaluates the maturation state of the 30S decoding state and couples this to the activation of its GTPase pocket and subsequent dissociation from the subunit such that the 30S maturation can continue.

ACCESSION NUMBERS

The electron density maps of the 30S–RsgA–GDPNP complex (RsgA-AI, RsgA-AI–S3 and RsgA-AI+S3) have been deposited in the 3DEM database with the accession codes EMD-3661, EMD-3662 and EMD-3663, respectively. The fitted coordinates for the 30S ribosomal subunit and RsgA have been deposited into the Protein Data Bank with the accession codes 5NO2, 5NO3 and 5NO4, respectively.

SUPPLEMENTARY DATA

Supplementary Data are available at NAR Online.

ACKNOWLEDGEMENTS

We thank the staff of Gene Research Center of Hirosaki University for the use of the facility. We are also grateful to Werner Kühlbrandt for his support throughout the project. Finally, we thank Diamond for access and support of the Cryo-EM facilities at the UK national electron bio-imaging centre (eBIC), proposal EM13322 (to S.C.), funded by the Wellcome Trust, MRC and BBSRC.

FUNDING

Japan Society for the Promotion of Science [23380054 to H.H., 19510229 to C.T.]; Hirosaki University Institutional Research (to H.H.); Bizkaia:Talent and the European Union's Seventh Framework Program (Marie Curie Actions, COFUND, to S.R.C., T.K.); Marie Curie Action Career Integration Grant [PCIG14-GA-2013-632072 to P.F.]; Ministerio de Economía Y Competitividad Grant [CTQ2014-55907-R to P.F., S.R.C.]; Human Frontiers Science Program Young Investigators Award [HFSP 67/07 to P.F., C.T.]. Funding for open access charge: Ministerio de Economía Y Competitividad Grant and Marie Curie Action Career Integration Grant.

Conflict of interest statement. None declared.

REFERENCES

1. Wilson,D.N. and Nierhaus,K.H. (2007) The weird and wonderful world of bacterial ribosome regulation. *Crit. Rev. Biochem. Mol. Biol.*, **42**, 187–219.
2. Mizushima,S. and Nomura,M. (1970) Assembly mapping of 30S ribosomal proteins from E. coli. *Nature*, **226**, 1214–1218.
3. Moazed,D., Stern,S. and Noller,H.F. (1986) Rapid chemical probing of conformation in 16 S ribosomal RNA and 30 S ribosomal subunits using primer extension. *J. Mol. Biol.*, **187**, 399–416.
4. Adilakshmi,T., Bellur,D.L. and Woodson,S.A. (2008) Concurrent nucleation of 16S folding and induced fit in 30S ribosome assembly. *Nature*, **455**, 1268–1272.
5. Talkington,M.W.T., Siuzdak,G. and Williamson,J.R. (2005) An assembly landscape for the 30S ribosomal subunit. *Nature*, **438**, 628–632.
6. Mulder,A.M., Yoshioka,C., Beck,A.H., Bunner,A.E., Milligan,R.A., Potter,C.S., Carragher,B. and Williamson,J.R. (2010) Visualizing ribosome biogenesis: parallel assembly pathways for the 30S subunit. *Science*, **330**, 673–677.
7. Sashital,D.G., Greeman,C.A., Lyumkis,D., Potter,C.S., Carragher,B. and Williamson,J.R. (2014) A combined quantitative mass spectrometry and electron microscopy analysis of ribosomal 30S subunit assembly in E. coli. *Elife*, **3**, e04491.
8. Ban,N., Beckmann,R., Cate,J.H., Dinman,J.D., Dragon,F., Ellis,S.R., Lafontaine,D.L., Lindahl,L., Liljas,A., Lipton,J.M. *et al.* (2014) ScienceDirectA new system for naming ribosomal proteins. *Curr. Opin. Struct. Biol.*, doi:10.1016/j.sbi.2014.01.002.
9. Xu,Z. and Culver,G.M. (2010) Differential assembly of 16S rRNA domains during 30S subunit formation. *RNA*, **16**, 1990–2001.
10. Soper,S.F.C., Dator,R.P., Limbach,P.A. and Woodson,S.A. (2013) In vivo X-ray footprinting of pre-30S ribosomes reveals chaperone-dependent remodeling of late assembly intermediates. *Mol. Cell*, **52**, 506–516.
11. Datta,P.P., Wilson,D.N., Kawazoe,M., Swami,N.K., Kaminishi,T., Sharma,M.R., Booth,T.M., Takemoto,C., Fucini,P., Yokoyama,S. *et al.* (2007) Structural aspects of RbfA action during small ribosomal subunit assembly. *Mol. Cell*, **28**, 434–445.
12. Dammel,C.S. and Noller,H.F. (1995) Suppression of a cold-sensitive mutation in 16S rRNA by overexpression of a novel ribosome-binding factor, RbfA. *Genes Dev.*, **9**, 626–637.
13. Daigle,D.M., Rossi,L., Berghuis,A.M., Aravind,L., Koonin,E.V. and Brown,E.D. (2002) YjeQ, an essential, conserved, uncharacterized protein from Escherichia coli, is an unusual GTPase with circularly permuted G-motifs and marked burst kinetics. *Biochemistry*, **41**, 11109–11117.
14. Himeno,H., Hanawa-Suetsugu,K., Kimura,T., Takagi,K., Sugiyama,W., Shirata,S., Mikami,T., Odagiri,F., Osanai,Y., Watanabe,D. *et al.* (2004) A novel GTPase activated by the small subunit of ribosome. *Nucleic Acids Res.*, **32**, 5303–5309.
15. Leipe,D.D., Wolf,Y.I., Koonin,E.V. and Aravind,L. (2002) Classification and evolution of P-loop GTPases and related ATPases. *J. Mol. Biol.*, **317**, 41–72.
16. Campbell,T.L., Daigle,D.M. and Brown,E.D. (2005) Characterization of the Bacillus subtilis GTPase YloQ and its role in ribosome function. *Biochem. J.*, **389**, 843–852.
17. Gibbs,M.R., Moon,K.-M., Chen,M., Balakrishnan,R., Foster,L.J. and Fredrick,K. (2017) Conserved GTPase LepA (Elongation Factor 4) functions in biogenesis of the 30S subunit of the 70S ribosome. *Proc. Natl. Acad. Sci. U.S.A.*, doi:10.1073/pnas.1613665114.
18. Hase,Y., Yokoyama,S., Muto,A. and Himeno,H. (2009) Removal of a ribosome small subunit-dependent GTPase confers salt resistance on Escherichia coli cells. *RNA*, **15**, 1766–1774.
19. Absalon,C., Hamze,K., Blanot,D., Frehel,C., Carballido-Lopez,R., Holland,B.I., van Heijenoort,J. and Séror,S.J. (2008) The GTPase CpgA is implicated in the deposition of the peptidoglycan sacculus in Bacillus subtilis. *J. Bacteriol.*, **190**, 3786–3790.
20. Campbell,T.L., Henderson,J., Heinrichs,D.E. and Brown,E.D. (2006) The yjeQ gene is required for virulence of Staphylococcus aureus. *Infect. Immun.*, **74**, 4918–4921.
21. Goto,S., Kato,S., Kimura,T., Muto,A. and Himeno,H. (2011) RsgA releases RbfA from 30S ribosome during a late stage of ribosome biosynthesis. *EMBO J.*, **30**, 104–114.
22. Thurlow,B., Davis,J.H., Leong,V., F Moraes,T., Williamson,J.R. and Ortega,J. (2016) Binding properties of YjeQ (RsgA), RbfA, RimM and Era to assembly intermediates of the 30S subunit. *Nucleic Acids Res.*, doi:10.1093/nar/gkw613.
23. Guo,Q., Yuan,Y., Xu,Y., Feng,B., Liu,L., Chen,K., Sun,M., Yang,Z., Lei,J. and Gao,N. (2011) Structural basis for the function of a small

GTPase RsgA on the 30S ribosomal subunit maturation revealed by cryoelectron microscopy. *Proc. Natl. Acad. Sci. U.S.A.*, **108**, 13100–13105.
24. Jeganathan,A., Razi,A., Thurlow,B. and Ortega,J. (2015) The C-terminal helix in the YjeQ zinc-finger domain catalyzes the release of RbfA during 30S ribosome subunit assembly. *J. Mol. Evol.*, doi:10.1261/rna.049171.114.
25. Jomaa,A., Stewart,G., Martín-Benito,J., Zielke,R., Campbell,T.L., Maddock,J.R., Brown,E.D. and Ortega,J. (2011) Understanding ribosome assembly: the structure of in vivo assembled immature 30S subunits revealed by cryo-electron microscopy. *RNA*, **17**, 697–709.
26. Bunner,A.E., Beck,A.H. and Williamson,J.R. (2010) Kinetic cooperativity in Escherichia coli 30S ribosomal subunit reconstitution reveals additional complexity in the assembly landscape. *Proc. Natl. Acad. Sci. U.S.A.*, **107**, 5417–5422.
27. Bourne,H.R., Sanders,D.A. and McCormick,F. (1991) The GTPase superfamily: conserved structure and molecular mechanism. *Nature*, **349**, 117–127.
28. Nichols,C.E., Johnson,C., Lamb,H.K., Lockyer,M., Charles,I.G., Hawkins,A.R. and Stammers,D.K. (2007) Structure of the ribosomal interacting GTPase YjeQ from the enterobacterial species Salmonella typhimurium. *Acta Crystallogr. Sect. F Struct. Biol. Cryst. Commun.*, **63**, 922–928.
29. Shin,D.H., Lou,Y., Jancarik,J., Yokota,H., Kim,R. and Kim,S.-H. (2004) Crystal structure of YjeQ from Thermotoga maritima contains a circularly permuted GTPase domain. *Proc. Natl. Acad. Sci. U.S.A.*, **101**, 13198–13203.
30. Voorhees,R.M. and Ramakrishnan,V. (2013) Structural basis of the translational elongation cycle. *Annu. Rev. Biochem.*, **82**, 203–236.
31. Mishra,R., Gara,S.K., Mishra,S. and Prakash,B. (2005) Analysis of GTPases carrying hydrophobic amino acid substitutions in lieu of the catalytic glutamine: implications for GTP hydrolysis. *Proteins*, **59**, 332–338.
32. Gulati,M., Jain,N., Anand,B., Prakash,B. and Britton,R.A. (2013) Mutational analysis of the ribosome assembly GTPase RbgA provides insight into ribosome interaction and ribosome-stimulated GTPase activation. *Nucleic Acids Res.*, **41**, 3217–3227.
33. Jomaa,A., Stewart,G., Mears,J.A., Kireeva,I., Brown,E.D. and Ortega,J. (2011) Cryo-electron microscopy structure of the 30S subunit in complex with the YjeQ biogenesis factor. *RNA*, **17**, 2026–2038.
34. Comartin,D. and Brown,E. (2006) Non-ribosomal factors in ribosome subunit assembly are emerging targets for new antibacterial drugs. *Curr. Opin. Pharmacol.*, **6**, 453–458.
35. Nikolay,R., Schmidt,S., Schlömer,R., Deuerling,E. and Nierhaus,K. (2016) Ribosome assembly as antimicrobial target. *Antibiotics*, **5**, 18.
36. Stokes,J.M., Davis,J.H., Mangat,C.S. and Williamson,J.R. (2014) Discovery of a small molecule that inhibits bacterial ribosome biogenesis. *Elife*, doi:10.7554/eLife.03574.001.
37. Daigle,D.M. and Brown,E.D. (2004) Studies of the interaction of Escherichia coli YjeQ with the ribosome in vitro. *J. Bacteriol.*, **186**, 1381–1387.
38. Li,X., Mooney,P., Zheng,S., Booth,C.R., Braunfeld,M.B., Gubbens,S., Agard,D.A. and Cheng,Y. (2013) Electron counting and beam-induced motion correction enable near-atomic-resolution single-particle cryo-EM. *Nat. Methods*, doi:10.1038/nmeth.2472.
39. Rohou,A. and Grigorieff,N. (2015) CTFFIND4: Fast and accurate defocus estimation from electron micrographs. *J. Struct. Biol.*, **192**, 216–221.
40. Scheres,S.H.W. (2012) RELION: Implementation of a Bayesian approach to cryo-EM structure determination. *J. Struct. Biol.*, **180**, 519–530.
41. DiMaio,F., Song,Y., Li,X., Brunner,M.J., Xu,C., Conticello,V., Egelman,E., Marlovits,T.C., Cheng,Y. and Baker,D. (2015) Atomic-accuracy models from 4.5-A cryo-electron microscopy data with density-guided iterative local refinement. *Nat. Methods*, **12**, 361–365.
42. Noeske,J., Wasserman,M.R., Terry,D.S., Altman,R.B., Blanchard,S.C. and Cate,J.H.D. (2015) High-resolution structure of the Escherichia coli ribosome. *Nat. Struct. Mol. Biol.*, doi:10.1038/nsmb.2994.
43. Brown,A., Long,F., Nicholls,R.A., Toots,J., Emsley,P. and Murshudov,G. (2015) Tools for macromolecular model building and refinement into electron cryo-microscopy reconstructions. *Acta Crystallogr. D Biol. Crystallogr.*, **71**, 136–153.
44. Emsley,P., Lohkamp,B., Scott,W.G. and Cowtan,K. (2010) Features and development of Coot. *Acta Crystallogr. D Biol. Crystallogr.*, **66**, 486–501.
45. Adams,P.D., Afonine,P.V., Bunkóczi,G., Chen,V.B., Davis,I.W., Echols,N., Headd,J.J., Hung,L.-W., Kapral,G.J., Grosse-Kunstleve,R.W. *et al.* (2010) PHENIX: a comprehensive Python-based system for macromolecular structure solution. *Acta Crystallogr. D Biol. Crystallogr.*, **66**, 213–221.
46. Afonine,P.V., Headd,J.J. and Terwilliger,T.C. (2013) New tool: phenix. real_space_refine. *Computational.*, **4**, 43–44.
47. Scheres,S.H.W. and Chen,S. (2012) Prevention of overfitting in cryo-EM structure determination. *Nat. Methods*, **9**, 853–854.
48. Kucukelbir,A., Sigworth,F.J. and Tagare,H.D. (2013) Quantifying the local resolution of cryo-EM density maps. *Nat. Methods*, **11**, 63–65.
49. Rosenthal,P.B. and Henderson,R. (2003) Optimal determination of particle orientation, absolute hand, and contrast loss in single-particle electron cryomicroscopy. *J. Mol. Biol.*, **333**, 721–745.
50. Mohan,S., Donohue,J.P. and Noller,H.F. (2014) Molecular mechanics of 30S subunit head rotation. *Proc. Natl. Acad. Sci. U.S.A.*, **111**, 13325–13330.
51. Kühlbrandt,W. (2014) Biochemistry. The resolution revolution. *Science*, **343**, 1443–1444.
52. Hussain,T., Llácer,J.L., Wimberly,B.T., Kieft,J.S. and Ramakrishnan,V. (2016) Large-scale movements of IF3 and tRNA during bacterial translation initiation. *Cell*, **167**, 133–137.
53. Kimura,T., Takagi,K., Hirata,Y., Hase,Y., Muto,A. and Himeno,H. (2008) Ribosome-small-subunit-dependent GTPase interacts with tRNA-binding sites on the ribosome. *J. Mol. Biol.*, **381**, 467–477.
54. López-Alonso,J.P., Fabbretti,A., Kaminishi,T., Iturrioz,I., Brandi,L., Gil-Carton,D., Gualerzi,C.O., Fucini,P. and Connell,S.R. (2016) Structure of a 30S pre-initiation complex stalled by GE81112 reveals structural parallels in bacterial and eukaryotic protein synthesis initiation pathways. *Nucleic Acids Res.*, doi:10.1093/nar/gkw1251.
55. Fischer,N., Neumann,P., Konevega,A.L., Bock,L.V., Ficner,R., Rodnina,M.V. and Stark,H. (2015) Structure of the E. coli ribosome-EF-Tu complex at <3 Å resolution by Cs-corrected cryo-EM. *Nature*, **520**, 567–570.
56. Fabbretti,A., Schedlbauer,A., Brandi,L., Kaminishi,T., Giuliodori,A.M., Garofalo,R., Ochoa-Lizarralde,B., Takemoto,C., Yokoyama,S., Connell,S.R. *et al.* (2016) Inhibition of translation initiation complex formation by GE81112 unravels a 16S rRNA structural switch involved in P-site decoding. *Proc. Natl. Acad. Sci. U.S.A.*, doi:10.1073/pnas.1521156113.
57. Demirci,H., Murphy,F., Belardinelli,R. and Kelley,A.C. (2010) Modification of 16S ribosomal RNA by the KsgA methyltransferase restructures the 30S subunit to optimize ribosome function. *RNA*, doi:10.1261/rna.2357210.
58. Demirci,H., Murphy,F., Murphy,E., Gregory,S.T., Dahlberg,A.E. and Jogl,G. (2013) A structural basis for streptomycin-induced misreading of the genetic code. *Nat. Commun.*, **4**, 1355.
59. Dong,J., Nanda,J.S., Rahman,H., Pruitt,M.R., Shin,B.-S., Wong,C.-M., Lorsch,J.R. and Hinnebusch,A.G. (2008) Genetic identification of yeast 18S rRNA residues required for efficient recruitment of initiator tRNA(Met) and AUG selection. *Genes Dev.*, **22**, 2242–2255.
60. Lancaster,L. and Noller,H.F. (2005) Involvement of 16S rRNA nucleotides G1338 and A1339 in discrimination of initiator tRNA. *Mol. Cell*, **20**, 623–632.
61. Noller,H.F., Hoang,L. and Fredrick,K. (2005) The 30S ribosomal P site: a function of 16S rRNA. *FEBS Lett.*, **579**, 855–858.
62. Voorhees,R.M., Schmeing,T.M., Kelley,A.C. and Ramakrishnan,V. (2010) The mechanism for activation of GTP hydrolysis on the ribosome. *Science*, **330**, 835–838.
63. Shetty,S. and Varshney,U. (2016) An evolutionarily conserved element in initiator tRNAs prompts ultimate steps in ribosome maturation. *Proc. Natl. Acad. Sci. U.S.A.*, doi:10.1073/pnas.1609550113.
64. Boehringer,D., O'Farrell,H.C., Rife,J.P. and Ban,N. (2012) Structural insights into methyltransferase KsgA function in 30S ribosomal subunit biogenesis. *J. Biol. Chem.*, **287**, 10453–10459.